RESEARCH PAPER

ECO-FRIENDLY SYNTHESIS OF ZINC OXIDE NANOPARTICLES ENCAPSULATED WITH AQUEOUS LEAF EXTRACT OF *NYCTANTHES ARBOR-TRISTIS* AND THEIR POTENTIAL FOR ENVIRONMENTAL REMEDIATION

Muskan[1], Meenakshi[1*], Amanjeet[2], Rahul Patwa[3] & Sonia[1]
[1] Department of Physics, Baba Mastnath University, Asthal Bohar, Rohtak, Haryana 124021, India
[2] Department of Physics, University of Delhi (Ramjas College), Delhi-110007, India
[3] Department of Physics, Chaudhary Ranbir Singh University, Jind, 126102, Haryana, India
*E-mail: meenakshi4phy@gmail.com

Abstract
The uncontrolled discharge of synthetic dyes from textile and allied industries into water bodies has emerged as a serious environmental concern, driving the urgent need for sustainable and effective wastewater treatment strategies. The present study reports an environmentally friendly technique for the synthesis of zinc oxide nanoparticles (ZnO NPs) using aqueous leaf extract of *Nyctanthes arbor-tristis* (NAT) and Zinc Nitrate as a precursor. NAT serves as a mild, natural and biocompatible agent that facilitates both the reduction and stabilization processes in nanoparticle formation, eliminating the requirement for external surfactants. Moreover, compounds produced as secondary metabolites are key contributors to the overall synthesis mechanism. High Resolution X-Ray Diffraction (HR-XRD) showed hexagonal wurtzite phase, accompanied by minimal tensile strain of 1.31×10^{-3}. GC-MS analysis confirmed the presence of various phytoconstituents associated with the surface of the ZnO-NAT nanoparticles. Optical and morphological characterization was carried out using ultraviolet-visible (UV-Vis) spectroscopy, photoluminescence (PL) and field-emission scanning electron microscopy **(**FESEM). The photocatalytic activity of Zinc oxide-*Nyctanthes arbor-tristis* nanoparticles (ZnO-NAT NPs) was investigated through methylene blue (MB) degradation initially in dark followed by Ultravoilet (UV) irradiated conditions in order to simulate practical wastewater treatment processes.

Keywords: Photoluminescence, Photocatalysts, Remediation, Metabolites, GC-MS
How to cite this article: Muskan, Meenakshi, Amanjeet, Rahul Patwa & Sonia. Eco-Friendly Synthesis Of Zinc Oxide Nanoparticles Encapsulated With Aqueous Leaf Extract Of Nyctanthes Arbor-Tristis And Their Potential For Environmental Remediation. Int J Drug Deliv Technol. 2026;16(77s):1747-1760. DOI: 10.25258/ijddt.16.77s.199.

Introduction

The rising demand from the textile industry has significantly enhanced the production of natural and artificial dyes. Annually, these dyes are produced in large quantity all over the world. It has been reported that the global production of dye is around 7×10^{8} tons annually. The dyes that are extensively used in clothing industries includes methylene blue (MB), aniline blue, toluidine blue, basic fuchsin, alcian blue, crystal violet, and Congo red. However, their substantial production has detrimental effect on the environment during printing, dyeing and finishing processes [1]. Most of these synthetic dyes are highly stable to temperature, water, chemical agents and hence, cannot be eliminated by conventional wastewater processes [2]. The release of untreated wastewater contaminate the water resources leading to scarcity of pure water as 1ppm of dye concentration in drinking water render it unsafe for human consumption. Moreover, the wastewater cause severe threat to crops and also causes carcinogenic, mutagenic, teratogenic effect to aquatic and other biotic components [3].

MB is a synthetic derivative that is considered an example of heterocyclic and aromatic organic chemicals. It behaves as an organic dye and pharmaceutical compound [4]. Its structure comprises benzene rings that consist of nitrogen and sulphur atom. This is a positively charged thiazine dye and is employed across various industrial sectors, such as food, cosmetics, and pharmaceuticals [5]. It is also utilized as colorants in industries such as textile, wool, silk, paper processing. This dye exhibits medicinal properties when dealt under controlled clinical conditions [6]. However, its uncontrolled exposure leads to contaminated water which is hazardous to ecosystem [7]. In humans, it can induce cardiovascular complications, cyanosis, vomiting, tissue necrosis, heinz body formation and jaundice [8]. Additionally, this dye has detrimental effects on plants and aquatic organisms. Therefore, the discharge of untreated or partially treated MB-containing effluents represents a serious environmental and public health concern, highlighting the urgent need for efficient remediation strategies prior to industrial discharge [9].

Various techniques have been employed for wastewater treatment such as ion exchange, chemical oxidation, adsorption, chemical precipitation and ion exchange [10]. Still, most of them have considerable drawbacks including use of harmful chemicals, need of elevated temperatures, significant cost implications, use of harmful chemicals, and generation of sludge [11]. Photocatalytic degradation is considered superior to other dye removal methods because it does not require additional chemicals and avoids formation of secondary pollutants [12]. As a result, it has attracted considerable attention due to their fascinating photocatalytic and catalytic reductive detoxification [13].

Recently, metal oxide NPs (MONPs) have grabbed significant insight as promising material for environmental remediation due to their outstanding photocatalytic activities [14]. MONPs allow photodegradation that decomposes organic pollutants into less toxic byproducts under ambient conditions [15]. Among the different types of MONPs, zinc oxide (ZnO) NPs have gained immense popularity because of band gap of 3.37 eV, due to high excitonic binding energy (60 meV), enhanced electron mobility (300 $cm^2\ V^{-1}\ s^{-1}$), high melting point (2248 K), and superior physicochemical stability [16]. Additionally, ZnO is considered a "generally safe" compound by the US Food and Drug Administration (21CFR182.8991), which makes it suitable for use not only in catalysis and environmental remediation but also in medical uses such as antimicrobial therapy, biosensing, and cancer therapy [17].

Numerous physicochemical techniques such as hydrothermal, microwave-assisted, thermal decomposition, plasma-assisted vapor deposition, and electrochemical synthesis can be used for NPs synthesis [18, 19]. However, these methods are usually energy-demanding, costly, and involve toxic and hazardous chemicals that produce environmentally hazardous by-products [20]. Moreover, the NPs prepared using these methods usually have low homogeneity and a high tendency to agglomerate [21]. On the other hand, green synthesis using biological materials such as plant extracts, microbes, fruits, leaves, seeds, and flowers has emerged as a sustainable and environmentally friendly method to nanoparticle synthesis [22]. In this approach, biological components serve as both stabilizer and reducing agents which facilitate the creation of homogenous and stable NPs [23].

Various studies have revealed that biogenically synthesized NPs possess higher biological and photocatalytic properties compared to those prepared using conventional methods [24]. For example, an increased antibacterial and photocatalytic property was observed for ZnO NPs prepared using Azadirachta indica [25], while the concentration of green extract has a significant effect on the biological and photocatalytic properties of ZnO NPs [26].

Various chemical and biogenic methods have been utilized for ZnO NPs synthesis. However, numerous conventional techniques still rely on toxic chemicals, need elevated temperatures, and lack comprehensive analysis. Most studies stop at FTIR analysis, which provides functional group data but fails to identify the specific molecular species bound to the nanoparticle surface. We bridge this analytical gap by employing GC-MS analysis to identify phytoconstituents associated with the surface of synthesized ZnO-NAT nanoparticles. To the best of our knowledge, such integration of green synthesis via *Nyctanthes arbor-tristis* leaf extract with advanced GC-MS analysis of synthesized sample has not yet been reported. Furthermore, efficient biogenic synthesis without the need for high-temperature calcination along with significant degradation of MB dye highlights the functional potential and novelty to the present investigation.

The present study focuses on eco-friendly, non-toxic and cost-effective approach for synthesis of Zinc oxide NPs encapsulated with NAT leaf extract. It also offer mechanistic insight into green synthesis through GC-MS by providing information about phytoconsituents present in ZnO-NAT NPs which act as strong capping and stabilizing agent. Moreover, PL, UV-Vis spectroscopy, FESEM and HR-XRD were also carried out for investigating optical and structural properties of as-synthesized NPs. The present work also reports ZnO-NAT NPs as a photocatalysts for photocatalytic degradation of MB dye in aqueous solution.

1. Methodology

1.1 Reagents and Materials

Analytical grade chemicals such as Zinc nitrate hexahydrate [$Zn(NO_3)_2 \cdot 6H_2O$; molecular weight 297.43 $g \cdot mol^{-1}$], Sodium hydroxide (NaOH), *N. arbor-tristis* (NAT) leaves, methylene Blue (MB) ($C_{16}H_{18}ClN_3S$) and double distilled water were used [27, 28, 29].

1.2 Collection and preparation of *N. arbor-tristis* (NAT) Leaf Extract

Fresh leaves of NAT were collected from village Kassar, Jhajjar, Haryana, India (28.701856° N latitude, 76.87511° E longitude), as per national and local guidelines (Fig.1) [30]. The washed leaves of

NAT were shade dried at room temp and grounded to uniform powder. 10 g leaf powder and double distilled water about 100 mL were stirred magnetically at 40 °C for 30 minutes. The mixture was centrifuged at 4000 rpm for 10 minutes, supernatant is the resulting aqueous NAT leaf extract [29, 31, 32].

Fig. 1 NAT incorporated for NPs fabrication

1.3 Green Synthesis of ZnO-NAT NPs

To synthesize a 0.2 M zinc precursor solution, 2.9748 g of zinc nitrate hexahydrate [$Zn(NO_3)_2 \cdot 6H_2O$] was added in 50 mL of deionized water under continuous magnetic stirring for 20 min (Fig.2).Subsequently, 50 mL of freshly prepared aqueous leaf extract of NAT was poured gradually to the zinc nitrate solution under constant stirring. The pH of the reaction mixture was set to 11 using an appropriate base solution. To facilitate nanoparticle formation, the mixture was then maintained at 70 °C for 4 h under continuous stirring. A noticeable change in color of the solution indicated the formation of ZnO-NAT NPs. The suspension was centrifuged at 4000 rpm for 10 min and then dried and ground to obtain ZnO-NAT NPs [29, 33, 34].

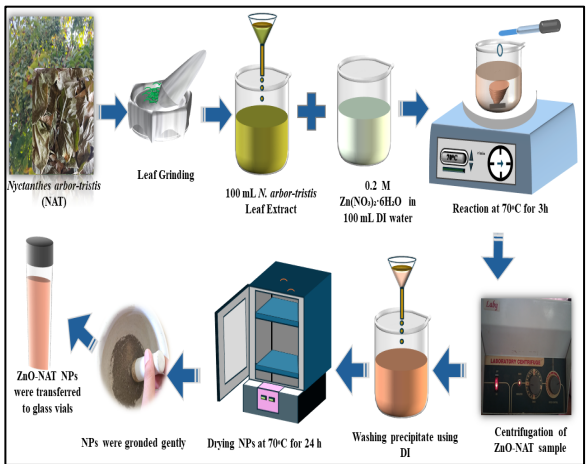

Fig.2 Schematic illustration of ZnO-NAT NPs synthesis

1.4 Characterization techniques

The predicted shape structure of prepared zinc oxide NPs was estimated by HR-XRD on a Rigaku SmartLab with Temperature-Dependent Testing Assembly with Cu Kα radiation (λ = 1.5405 Å). Diffraction data were recorded from 20° to 80° (2θ) at a scan rate of 0.02°/s [35]. UV-Visible spectroscopy (Agilent Cary 5000) was utilized to affirm the formation of ZnO-NA NPs and study their optical behavior. PL measurement was carried out on a luminescence spectrophotometer WiTech alpha 300R, made in Germany (325 nm) using He-Cd laser with excitation wavelength at 325 nm. Surface morphology was detected using a Gemini SEM 500 Field-emission scanning electron microscopy (FESEM). A Nicolet iS50 spectrophotometer was used to perform FTIR analysis in order to identify functional groups. These characterizations were carried out at the University Science Instrumentation Centre (USIC), University of Delhi, New Delhi. GC-MS analysis was carried out at the Central Instrumentation Laboratory, Central University of Punjab (CUPB), Ghudda, Bathinda, using a GCMS-TQ8040 instrument (Shimadzu, Japan). Prior to analysis, the synthesized ZnO-NAT nanoparticle powder was dispersed in methanol to facilitate the release and detection of nanoparticle-associated organic constituents. The resulting methanolic dispersion was subjected to GC-MS analysis. Separation was achieved using an RTX-5MS capillary column (30 m × 0.25 mm × 0.25 µm film thickness) with helium as the carrier gas. The resulting compounds were identified by comparing their retention indices and mass spectral patterns with those listed in National Institute of Standards and Technology (NIST14) collection [36, 37 38].

1.5 Dye catalytic experiment

The photocatalytic activity of ZnO-NAT NPs was evaluated using methylene blue dye in an aqueous medium. MB dye solutions (10 mg/L) were prepared in deionized water and for calibration, a series of standard MB solutions with varying concentrations were prepared, and their absorbance values were measured using Vis spectrophotometer to obtain a calibration curve [39]. For the photocatalytic study, 20 mg of ZnO-NAT NPs were dispersed in 50 mL of MB solution prepared from the stock. The initial absorbance (A_0) was recorded before light illumination. The mixture was then stirred in dark conditions for 60 minutes to establish equilibrium state before light exposure. Also, prior to light

illumination, the suspension was maintained under dark conditions with continuous stirring for 60 min so that equilibrium between the dye molecules and surface of catalyst can be attained. After achieving equilibrium, the solution was exposed to blue light source for 240 minutes. At regular intervals of 30 minutes, 3 mL aliquots were withdrawn and centrifuged at 5000 rpm for 5 minutes to separate the catalyst particles.

The collected supernatant was analyzed via visible spectrophotometer to obtain absorbance (A_t). Variations in absorbance were used to assess dye degradation rate. The role of concentration and exposure time on degradation was also investigated, and efficiency (%) was calculated using the stated equation (1) [39, 40].

$$\text{Degradation Efficiency (\%)} = \frac{C_0 - C_t}{C_0} \times 100 \quad \textbf{(1)}$$

where, C_0 represents the initial concentration of dye and C_t denotes the dye concentrations at time t, respectively [39].

2. Results

2.1 HR-XRD Analysis

HR-XRD was used to examine the crystal structure of the as-synthesised sample. The NPs were scanned from 20° to 80° at 2θ. The diffraction pattern highlighted in Fig. 3(a) confirmed the crystalline structure of the synthesized nanoparticles as well as the purity of the sample. The sharp peaks indicate the crystallinity of the nanoparticles.

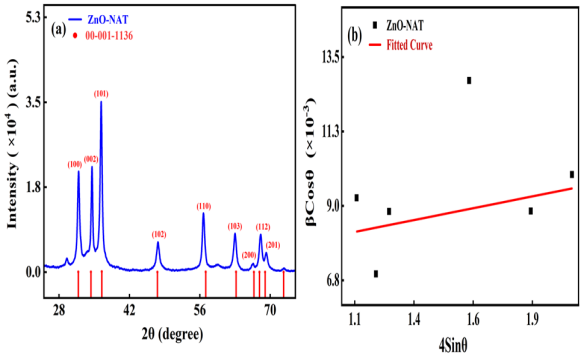

Fig. 3(a) HR-XRD profile for ZnO-NAT NPs. **(b)** shows W-H Plot

The HR-XRD pattern exhibits peaks at (100), (002), (101), (102), (110), (103), (200), (112), (201) and (004), which align perfectly with the hexagonal wurtzite phase of ZnO (JCPDS Card No. 00-001-1136) [41]. The purity of the sample was confirmed no secondary phases or impurity-related peaks were detected. The average size of the as-synthesized sample as determined by Debye-Scherrer equation (2) [40], is 20.45 nm.

$$D = \frac{K\lambda}{\beta \cos\theta} \quad \textbf{(2)}$$

D is the value of crystallite size in nanometers, β is the relevant plane's FWHM in radians, θ represents diffraction angle, K denotes Scherrer's constant (typically 0.9) and λ denotes X- ray radiation's wavelength, which is commonly used as 0.154 nm.

$$Dislocation\ Density = \frac{1}{D^2} \quad \textbf{(3)}$$

Thereafter, using equation (3) [40] the dislocation density of ZnO-NAT NPs is 4.33×10^{15} m^{-2}.

2.1.1 Microstrain Evaluation using Williamson-Hall (W-H) Plot

The lattice strain of the NPs was assessed by utilizing the W-H plot method as depicted in Fig.3(b), and the corresponding values are summarized in Table 1. Both macro-strain and crystallite size influences the peak broadening in the HR-XRD data.

In particular, the broadening can be divided into two components: βE, which is the result of deformation broadening, and βD, that derive from grain size broadening. Equation (4) [40] can be employed to determine βt, which represents the total peak broadening.

$$\beta_T = \frac{k\lambda}{D \times \text{Cos}\theta} + 4\varepsilon \times \tan\theta \quad \textbf{(4)}$$

Here, ε indicates the lattice strain. The relationship can be written in a linear form, where kλ/D represents the y-intercept and ε is the slope of the line given by equation (5) [35, 40].

$$\beta_T \times Cos\theta = \varepsilon(4Sin\theta) + \frac{k\lambda}{D} \quad \textbf{(5)}$$

Figure 3 depicts the W-H curve for ZnO-NAT NPs which illustrate the correlation between 4sinθ and βcosθ. The data was analyzed via linear regression, where the slope of the fitted line provides the value for the lattice strain [40].

Table 1: Crystallographic parameters of ZnO-NAT NPs

Nanoparticles	**ZnO-NAT NPs**
Crystallite Size (debye scherrer	15.19 nm

method)	
Dislocation Density	4.33×10^{15} m^{-2}
Crystallite Size(W-H Plot)	20.45 nm
Strain	1.31×10^{-3}

The plot's slope and intercept were found to be 0.0013 and 0.00678, respectively. As shown in Table 1, the crystallite size was 20.45 nm, and the corresponding tensile strain (ε) was estimated to be 1.31×10^{-3}. These observations align with previous findings [35, 31].

3.3 GC-MS Analysis

The GC-MS chromatogram of the biosynthesized ZnO-NAT NPs is shown in Fig. 4, while the identified compounds are summarized in Table 2 [36]. The chromatogram displays distinct and well-resolved peaks in the retention time (RT) range of ~13-32 min, confirming the presence of diverse organic constituents associated with the nanoparticle surface.

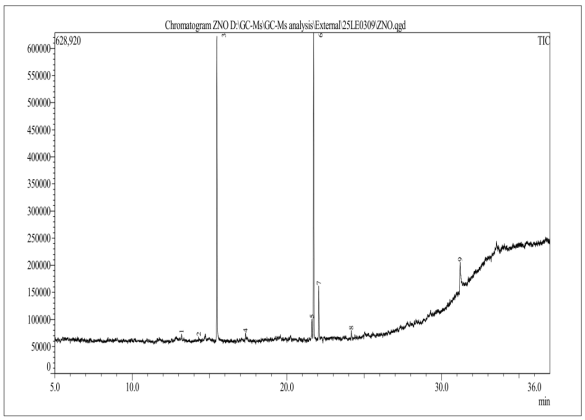

Fig.4: GC-MS chromatogram of ZnO-NAT NPs displayed the presence of 2,4-Di-tert-butylphenol, Hexadecanoic acid, methyl ester, Benzenepropanoic acid, 3,5-bis(1,1-dimethylethyl)-4-hydroxy-, Heptadecanoic acid, 16-methyl-, methyl ester, 13-Docosenamide, (Z)-

Table 2: GC-MS analysis of green-mediated ZnO-NAT NPs

Peak No.	**IUPAC name**	**RT(min)**	**Area**	**Area%**	**Molecular weight**	**Formula**
3	2,4-Di-tert-butylphenol	15.473	12750166	39.97	206	$C_{14}H_{22}O$
5	Hexadecanoic acid, methyl ester	21.615	83902	2.63	270	$C_{17}H_{34}O_2$
6	Benzenepropanoic acid, 3,5-bis(1,1-dimethylethyl)-4-hydroxy-	21.728	1284218	40.26	292	$C_{18}H_{28}O_3$
8	Heptadecanoic acid, 16-methyl-, methyl ester	24.168	38836	1.22	298	$C_{19}H_{38}O_2$
9	13-Docosenamide, (Z)-	31.200	188172	5.90	337	$C_{22}H_{43}NO$

The identified compounds are attributed to phytochemical constituents associated with the surface of ZnO-NAT nanoparticle, indicating the

presence of organic molecules retained during the green synthesis process. The GC-MS analysis showed five major compounds associated with the ZnO-NAT nanoparticles (Fig. 4). The compounds were identified from their retention times and fragmentation patterns in the mass spectra. The results showed that benzenepropanoic acid, 3,5-bis(1,1-dimethylethyl)-4-hydroxy- (40.26%) and 2,4-di-tert-butylphenol (39.97%) were the main compounds identified in the sample. Further, fatty acid derivatives like hexadecanoic acid methyl ester (2.63%) and heptadecanoic acid methyl ester (1.22%) were also detected and may contribute in capping and stabilizing the nanoparticles. The presence of 13-docosenamide (Z-) (5.90%) (Table 2) also supports the mechanism of stabilization by surface adsorption. The results of GC-MS agreed the previous findings which uncovered the presence of various phytochemicals associated with biosynthesized ZnO-NAT NPs. These biomolecules facilitate the conversion of zinc precursor into ZnO-NAT NPs and prevent particle agglomeration by stabilizing the nanoparticle surface [29].

3.4 UV-Vis Spectroscopy

UV-Vis absorption spectroscopy was utilized to examine the optical characteristics of semiconductor NPs. This technique is commonly employed to investigate material absorption behavior.

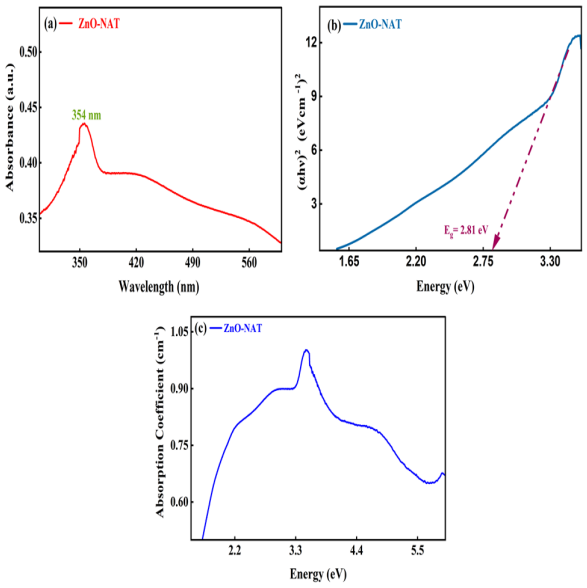

Fig. 5 (a) UV- visible absorbance spectrum for ZnO-NAT NPs, **(b)** Band gap determination via tauc plot, **(c)** UV- visible absorption coefficient of ZnO-NAT NPs

Fig.5(a) illustrates the UV-Vis absorption profile and (b) corresponds to Tauc plot of the synthesized ZnO-NAT NPs, within 200-800 nm range. A prominent absorption peak appeared at 354 nm that confirmed synthesis of ZnO-NAT NPs. The measured wavelength is shorter than the characteristic absorption wavelength of bulk ZnO which is usually 380 nm [42]. The peak position reflects a blue shift in excitonic absorption [43]. Similar absorbance peaks (λ_{max}) had been reported by other researchers [29]. Fig. 5 (c) illustrates the relationship between the absorption coefficient (α) and photon energy (hv) for ZnO-NAT NPs. The absorption coefficient was determined using Equation (6) [40] yielding significant insights into the optical characteristics of the material.

$$\alpha = \frac{2.303\,A}{t} \quad \textbf{(6)}$$

The absorption coefficient is low at lower photon energies and increases gradually, indicating weak absorption due to defect states. At shorter wavelengths (higher energies), it rises sharply and reaches a maximum near the band gap region, demonstrating strong intrinsic absorption of ZnO-NAT NPs in the UV region. Depending on the crystalline structure, band gap energy is a crucial factor in determining wavelengths of material. According to the Tauc equation provided by equation (7) [31], the band gap for ZnO-NAT NPs was estimated to be 2.81 eV by extrapolating the linear region of the absorption edge. In this case, A denotes the empirical constant, "E_g" for band gap energy, hv stands for photon energy, and considering zinc oxide as a direct band gap semiconductor, γ = ½.

$$(\alpha h\nu)^{1/\gamma} = A\,(h\nu - E_g) \quad \textbf{(7)}$$

The reduction in the optical band gap may be attributed to phytochemical constituents originating from the plant extract, which cap and modify the nanoparticle surface, thereby introducing localized defect states [44]. Generally, biosynthesized nanoparticles exhibit enhanced reactivity compared to their chemically or physically synthesized counterparts [45, 46]. The present study shows close resemblance with the report [47] that indicated an optical band of 2.67 eV with an absorption edge near 375 nm for zinc oxide NPs employing *Eucalyptus globulus* leaf extract.

3.5 Photoluminescence Study

To investigate the optical characteristics of the ZnO-NAT sample, PL spectra was recorded at room temperature using a 325 nm excitation source is shown in Fig.6. The emission spectrum exhibits both ultraviolet and visible emission bands, indicating the presence of intrinsic defects and excitonic recombination processes.

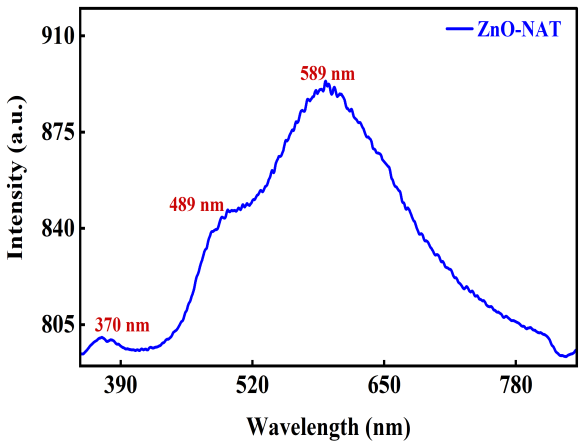

Fig.6 PL spectrum of ZnO-NAT NPs

A low-intensity near band edge (NBE) emission peak appears at around 370 nm, which is responsible for radiative recombination of free excitons in ZnO. This UV emission confirms the good crystalline nature of the synthesized ZnO-NAT NPs. However, the relatively low intensity of this peak suggests that defect-mediated transitions dominate over direct band-to-band recombination. The PL spectrum further shows a broad and intense emission band in the visible region, indicating the presence of deep-level defect states within the band gap of ZnO. The blue emission peak at 486 nm is attributed to intrinsic defects such as zinc interstitials (Zn_i) and oxygen vacancies (V_o), which create shallow donor energy levels below the conduction band. The radiative transition from these defect states to the valence band gives rise to the observed blue emission. The dominant emission peak at 589 nm, located in the yellow region, is associated with deep-level defects, mainly oxygen vacancies and oxygen interstitials. The strong intensity of this emission indicates a high concentration of oxygen-related defects in the ZnO lattice. These defects are introduced during the green synthesis process due to the interaction of phytochemicals present in the leaf extract.

Visible emission in ZnO is mostly attributed to intrinsic point defects, including zinc interstitials, zinc vacancies, oxygen interstitials, and oxygen vacancies, which generate deep energy levels within the band gap. These defect states prolong the lifespan of charge carriers by serving as sites for trapping and suppressing direct recombination of photogenerated charge carriers. Furthermore, these defects serve as active sites for photocatalysis.

Under blue light, the photogenerated electrons and holes under redox conditions migrate towards the surface of ZnO-NAT NPs and then facilitate the formation of oxidative species such as hydroxyl (•OH) and superoxide radicals (O_2•-) radicals [36]. These highly reactive intermediates greatly enhance photocatalytic performance by aiding in the degradation of organic contaminants. Therefore, the strong visible emission confirms the defect-rich nature of ZnO-NAT NPs. Thus, PL study clearly demonstrates that the weak UV emission corresponds to excitonic recombination, strong visible emission originates from defect-related deep levels and defect-rich nature of ZnO-NAT NPs is highly favorable for photocatalytic and environmental remediation applications [40].

3.6 FTIR analysis

Fig. 7 illustrates that FTIR characterization carried out to determine the functional groups responsible for NPs formation. The analysis was examined in the range of 400-4000 cm^{-1}. The nanoparticles exhibit a variety of absorption peaks at 3448.1, 1492.6, 1400.1, 1029.8, 908.3, and 871.7 cm^{-1}, along with a characteristic Zn–O vibration in the low-wavenumber region.

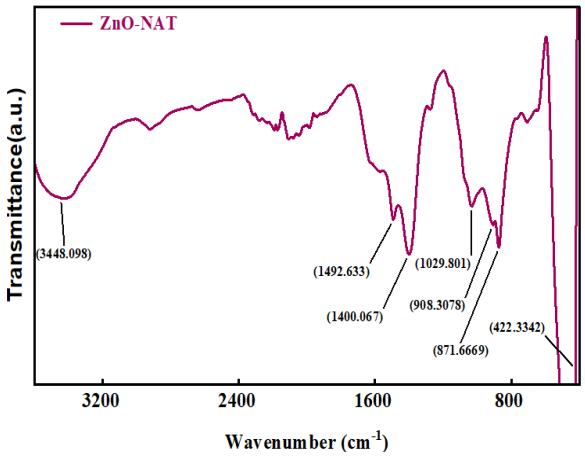

Fig.7 FTIR spectra of ZnO-NAT NPs

A broad absorption band observed at 3448.1 cm^{-1} represents O–H stretching vibrations which originates from phenolic compounds and alcohols present in the plant extract, suggests the presence of

surface-absorbed water and hydroxyl groups. The presence of these hydroxyl groups suggests the adsorption of phytochemical constituents on the nanoparticle surface. The bands at 1492.6 cm^{-1} and 1400.1 cm^{-1} are assigned to C–N stretching or aromatic C=C vibrations, that indicates the involvement of proteins or amino compounds in nanoparticle stabilization. The absorption band at 1029.8 cm^{-1} and 908.3 cm^{-1} are associated with C–O stretching vibrations of alcohols, ethers, or esters. These oxygen-containing groups improve the adsorption of reactant molecules on the nanoparticle surface, which is a crucial step in photocatalytic reactions. The existence of organic capping agents that can alter surface characteristics and improve catalytic interactions is further confirmed by the peak detected at 871.7 cm^{-1}, which corresponds to out-of-plane bending vibrations of aromatic C–H bonds. Zn–O stretching vibrations are responsible for a prominent and distinctive absorption band at 441.2 cm^{-1}, indicating the successful production of ZnO nanoparticles. This band is closely linked to the metal-oxygen lattice, lattice and provides evidence for the formation of crystalline ZnO nanoparticles [40, 42]

3.7 FESEM Analysis

The micrographs for ZnO-NAT NPs revealed spherical to quasi- spherical morphology with aggregation present in some clusters of spheres, as described in literature. The shape and size distribution of the biosynthesized ZnO-NAT nanoparticles were analyzed using FESEM, as illustrated in Fig. 8. The morphology and particle size distribution of the biologically as-synthesized ZnO-NAT NPs were examined using FESEM, as shown in Fig.8. At lower magnification, the nanoparticles are seen to be relatively uniformly distributed, indicating homogeneous nucleation and growth. With increasing magnification, the surface features become more distinct, revealing clusters of fine nanograins forming larger aggregated structures with rough textures. The corresponding particle size distribution histograms exhibit near-Gaussian behavior, indicating a fairly uniform particle size distribution with moderate polydispersity. The analysis was conducted at magnification at 50.23 KX, 75.34 KX and 100.28 KX had demonstrated particle sizes in the range of approximately 211.22-230.4 nm for ZnO-NAT NPs.

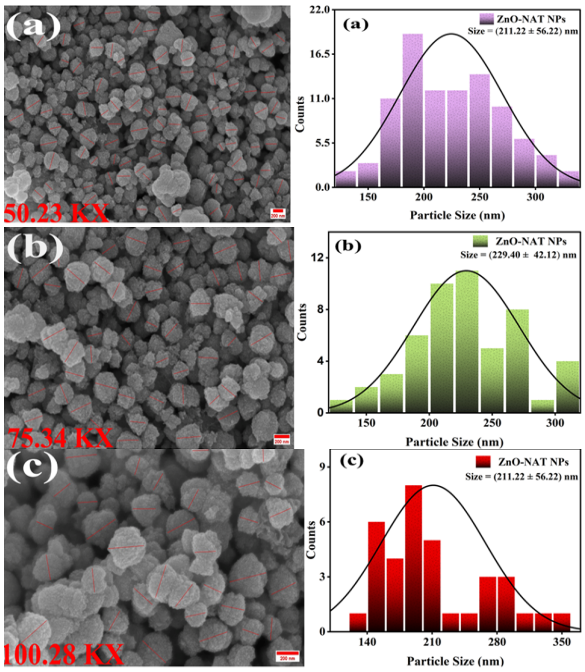

Fig. 8 FESEM micrographs illustrating ZnO-NAT NPs at magnifications **(a)** 50.23 KX, **(b)** 75.34KX, **(c)** 100.28 KX, and their particle size distribution histograms

It is clear that nanoparticles get severely aggregated leading to larger particle size formation. This agglomeration and clustering of nanoparticles may be attributed to the inherently high surface energy of ZnO nanoparticles along with the influence of phytochemicals acting as stabilizing agents during biogenic synthesis process. The diameter of ZnO-NAT NPs measured by FESEM is larger than the crystallite size determined via XRD (Scherer and W-H calculations), that are consistent with micrographs reported in literature [31,48,49]. This indicates that the ZnO-NAT NPs are polycrystalline since each nanoparticle has several tens of crystallite grains with a diameter of about 15 nm that are consistent with peaks reported in literature study [48, 49].

3.8 Photocatalytic degradation of MB dye

The photocatalytic efficiency of ZnO-NAT NPs was evaluated by degradation of MB under blue light. The corresponding UV-Visible absorption spectra recorded at different irradiation times are shown in Fig. 9(a). MB showed an intense absorption peak at 664 nm initially. With increasing exposure time showed gradual decrease in intensity on exposure to blue light.

For the control, the degradation of MB concentration in the dark phase showed a slight reduction in MB concentration due to adsorption of dye onto ZnO-NAT NPs. After 60 min, the blue light was switched on and a gradual decrease in absorbance was recorded with increasing irradiation time, indicating effective photocatalytic activity. The initial absorbance (A_0) of MB was 1.209 corresponding to an initial concentration (C_0) of 10.1 mg/L. The concentration of MB decreased progressively from 7.38 mg/L at 30 min to 2.03 mg/L at 240 min. The degradation efficiency reached 80% after 240 min of irradiation showed in Fig.9 confirming the photodegradation of MB dye [39].

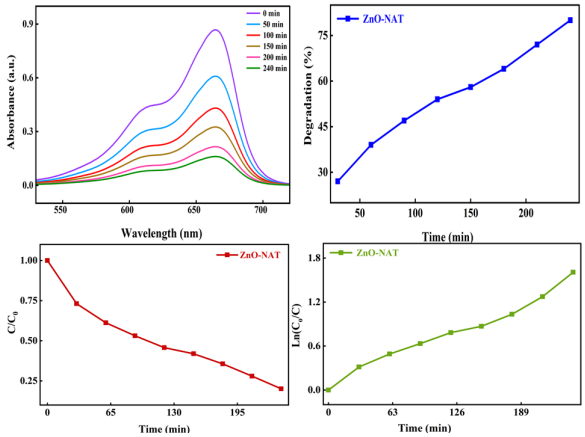

Fig. 9- (a) UV-Visible absorption spectra for MB at different irradiation time ,(b) Photocatalytic degradation efficiency (%) of MB dye as a function of irradiation time using ZnO-NAT NPs, (c) Variation of C/C_0 with irradiation time, and (d) Pseudo-first-order kinetic plot of $\ln(C_0/C)$ versus irradiation time for MB degradation

Table 3: Comparative photocatalytic performance of ZnO-NAT NPs synthesized via different green and chemical routes for MB degradation under various light irradiation conditions

S. No.	**Synthesis route/ source for ZnO synthesis**	**Model Pollutant**	**Process type/Light source**	**Degradation (%)**	**Time (min)**	**DOI / Reference**
1.	*Citrus Limetta rind* pulp (U-CLRP) extract	MB	Visible light radiation. UV irradiation	57 74	210	[50]
2.	*C. paradisi* fruit peel extract	MB	Sunlight/ photocatalysis	56	360	[51]
3.	Co-precipitation technique	MB	Sunshine	62	90	[52]
4.	*Musa Acuminata* Peel Extract/ sol-gel metho	MB	Visible light	57	60	[53]

	d					
5.	Combustion synthesis method	MB	Sunlight	43.58	75	[54]
6.	NAT leaf extract	MB	Visible light	80	240	Present study

To determine the reaction rate constant (k), the degradation data were analyzed using the pseudo-first-order kinetic model expressed as in equation (8) [55], where C_t represents the concentration of MB at different irradiation times and C_o represents the initial concentration of MB solution.

$$ln\left({C_o}/{C_t}\right) = kt \quad \textbf{(8)}$$

The photocatalytic degradation obeys first-order reaction kinetics, as shown by the linear correlation between ln(C_0/Ct) and exposure time in Fig. 9(c). The calculated rate constant (k) further confirms the efficient photocatalytic performance of ZnO-NAT NPs under blue light irradiation. The rate constant (k) for the photodegradation of MB via ZnO-NAT NPs was calculated to be 0.0067 min^{-1} based on the slope of the linear plot [56].

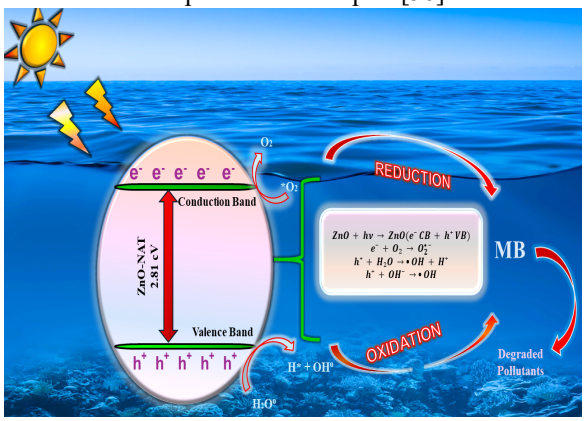

Fig. 10 Schematic illustration of the photocatalytic process involved in the degradation of MB

Fig.10 illustrates the mechanism of MB dye degradation in the presence of ZnO-NAT NPs. The photodegradation behavior of ZnO NPs has already been widely reported in earlier studies (Table 3). The photodegradation mechanisms that result in the formation of of CO_2 and H_2O as byproducts are outlined in the following equations (9 -13) based on previous investigations [57].

$$ZnO + h\nu \rightarrow ZnO(e^- CB + h^+ VB) \quad \textbf{(9)}$$

$$e^- + O_2 \rightarrow O_2^{\bullet -} \quad \textbf{(10)}$$

$$h^+ + H_2O \rightarrow \bullet OH + H^+ \quad \textbf{(11)}$$

$$h^+ + OH^- \rightarrow \bullet OH \quad \textbf{(12)}$$

$$\bullet OH \,/\, O_2^{\bullet -} + MO \rightarrow degradation\ products \rightarrow CO_2 + H_2O \quad \textbf{(13)}$$

In ZnO-NAT NPs, incident photons possessing energy equal to or greater than the bandgap, transfer of electrons from the lower-energy band (VB) to the higher-energy band(CB) produces paired charge carriers (e^-/h^+) [57]. The superoxide radicals ($O_2\bullet^-$) are formed when photo-generated electrons reduce molecular oxygen adsorbed on the ZnO surface. The holes in the valence band produce hydroxyl radicals (•OH) by facilitating the oxidation of surface hydroxyl groups (OH^-) or water molecules (H_2O). The radicals (•OH and $O_2\bullet^-$) breaks down the conjugated structure of MB that results into CO_2, H_2O, and less poisonous byproducts [57].

4 Conclusion

The present work highlights the synthesis of ZnO-NAT NPs via biogenic route. Also, its structural, optical and morphological characteristics are thoroughly evaluated. HR-XRD confirmed the hexagonal wurtzite structure of ZnO-NAT NPs with an average crystallite size of 15.19 nm. Through W-H Analysis, lattice strain of 1.31×10^{-3} with 4.33×10^{15} m^{-2} of dislocation density suggest good crystallinity with minimal defects. Optical studies employing UV-Vis spectroscopy showed strong absorption peak at 354 nm which corresponds to an estimated band gap of 2.81 eV. PL analysis points towards the defects states in ZnO-NAT NPs that effectively suppress

recombination rates. FESEM micrographs show spherical to quasi spherical shape of the particles. ZnO-NAT NPs acted as efficient photocatalysts as it degrade 80% of MB dye within 240 minutes of exposure to blue light. Such performance underscores the potential of the NPs as robust tools for remediating environmental pollutants.

Acknowledgments: The authors appreciate technical support provided by Baba Mastnath University, Asthal Bohar, Rohtak and Research Lab, Dept. of physics, Ramjas college in completing the research work. The authors are also grateful to University Science Instrumentation Centre (USIC), University of Delhi, New Delhi for research characterization.

Author Contributions: Muskan: Writing – original draft, Writing – review and editing, Data curation, Methodology, Visualization, Meenakshi: Supervision, Formal analysis, Amanjeet: Supervision, Investigation, Formal analysis, Resources, Rahul: Validation, Data curation, Methodology, Sonia: Formal analysis

Data availability: The datasets generated and/or analyzed during the current study are not publicly available because they are private, but are available from the corresponding author on reasonable request.

Declaration of Interests:

Competing interests: The authors declare that they have no known competing financial interests or personal relationships that could have appeared to influence the work reported in this paper.

Consent for publication: All authors accepted the publication of the manuscript in the present form.

Funding: The authors declare that no funds, grants, or other support were received during the preparation of this manuscript.

References

[1] P.O. Oladoye, T.O. Ajiboye, E.O. Omotola, O.J. Oyewola, Methylene blue dye: Toxicity and potential elimination technology from wastewater, Results in Engineering 16 (2022) 100678. https://doi.org/10.1016/j.rineng.2022.100678

[2] G. Bal, A. Thakur, Distinct approaches of removal of dyes from wastewater: A review, Mater. Today Proc. 50 (2022) 1575–1579. https://doi.org/10.1016/j.matpr.2021.09.119

[3] S. Modi, V.K. Yadav, A. Gacem, I.H. Ali, D. Dave, S.H. Khan, K.K. Yadav, S. Rather, Y. Ahn, C.T. Son, Recent and emerging trends in remediation of methylene blue dye from wastewater by using zinc oxide nanoparticles, Water (Basel). 14 (2022) 1749. https://doi.org/10.3390/w14111749

[4] A.G. Braish, A.F. Hassan, S.A. El-Essawy, M.M.T. El-Tahawy, Fabrication of nanozeolite-Y/chitosan composite based on rice husks for efficient adsorption of methylene blue dye: kinetic and thermodynamic studies, Adsorption 30 (2024) 1643–1661. https://doi.org/10.1007/s10450-024-00527-x

[5] S.O. Fakayode, C. Lisse, W. Medawala, P.N. Brady, D.K. Bwambok, D. Anum, T. Alonge, M.E. Taylor, G.A. Baker, T.F. Mehari, Fluorescent chemical sensors: applications in analytical, environmental, forensic, pharmaceutical, biological, and biomedical sample measurement, and clinical diagnosis, Appl. Spectrosc. Rev. 59 (2024) 1–89. https://doi.org/10.1080/05704928.2023.2177666

[6] I. Khan, K. Saeed, I. Zekker, B. Zhang, A.H. Hendi, A. Ahmad, S. Ahmad, N. Zada, H. Ahmad, L.A. Shah, Review on methylene blue: its properties, uses, toxicity and photodegradation, Water (Basel). 14 (2022) 242. https://doi.org/10.3390/w14020242

[7] A. Saravanan, Y.P. Ragini, P.S. Kumar, P. Thamarai, G. Rangasamy, A critical review on the removal of toxic pollutants from contaminated water using magnetic hybrids, Environmental Science and Pollution Research 30 (2023) 105099–105118. https://doi.org/10.1007/s11356-023-29811-z

[8] B.H. Hameed, A.L. Ahmad, K.N.A. Latiff, Adsorption of basic dye (methylene blue) onto activated carbon prepared from rattan sawdust, Dyes and Pigments 75 (2007) 143–149.https://doi.org/10.1016/j.dyepig.2006.05.039

[9] F. Gull, R. Riaz, K. Ansari, H. Atiq, Examining the photo catalytic potency of annealed and un-annealed ZnO and nickel doped ZnO for degradation of organic pollutants in waste waters, Sci. Rep. 14 (2024) 21828. https://doi.org/10.1038/s41598-024602585

[10] I. Zinicovscaia, Conventional methods of wastewater treatment, Cyanobacteria for Bioremediation of Wastewaters (2016) 17–25. https://doi.org/10.1007/978-3-319-26751-7_3

[11] F.P. Camargo, P. Sérgio Tonello, A.C.A. dos Santos, I.C.S. Duarte, Removal of toxic metals from sewage sludge through chemical, physical, and biological treatments—a review, Water Air Soil Pollut. 227 (2016)

433. https://doi.org/10.1007/s11270-016-3141-3

[12] H. Kumari, Sonia, Suman, R. Ranga, S. Chahal, S. Devi, S. Sharma, S. Kumar, P. Kumar, S. Kumar, A review on photocatalysis used for wastewater treatment: dye degradation, Water Air Soil Pollut. 234 (2023) 349. https://doi.org/10.1007/s11270-023-06359-9

[13] M. Naz, A. Rafiq, M. Ikram, A. Haider, S.O.A. Ahmad, J. Haider, S. Naz, Elimination of dyes by catalytic reduction in the absence of light: A review, J. Mater. Sci. 56 (2021) 15572–15608. https://doi.org/10.1007/s10853-021-06279-1

[14] D.J.G. Dabodabo, C.J.H. Solidor, Metal Oxide Nanoparticles for Various Applications, in: Carrageenan-Mediated Green Synthesis of Metal Oxide Nanoparticles for Various Applications, CRC Press, 2025: pp. 71–88.

[15] R. Neelancherry, M. Kumar, Nanotechnology in Wastewater Treatment, (2025). https://doi.org/10.1007/978-3-031-94246-4

[16] P. Kumari, A. Srivastava, R.K. Sharma, D. Sharma, S.K. Srivastava, Zinc oxide: a fascinating material for photovoltaic applications, in: Nanomaterials for Innovative Energy Systems and Devices, Springer, 2022: pp. 173–241. https://doi.org/10.1007/978-981-19-0553-7_6

[17] A. Molla, H. Akhter, E.I. Rafi, A. Islam, E.P. Lipy, M.A.S. Miah, S. Islam, Phytochemical Profiling, Molecular Docking, ADMET Analysis of Zingiber Officinale Peel Extract for the Biogenic Synthesis of ZnO and Fe-Doped ZnO Nanoparticles with Antibacterial and Photocatalytic Potential, ACS Omega 10 (2025) 59849–59871. https://doi.org/10.1021/acsomega.5c09902

[18] G.N. Kokila, C. Mallikarjunaswamy, V.L. Ranganatha, A review on synthesis and applications of versatile nanomaterials, Inorganic and Nano-Metal Chemistry 54 (2024) 942–971. https://doi.org/10.1080/24701556.2022.2081189

[19] A. Miri, F. Mahabbati, A. Najafidoust, M.J. Miri, M. Sarani, Nickel oxide nanoparticles: biosynthesized, characterization and photocatalytic application in degradation of methylene blue dye, Inorganic and Nano-Metal Chemistry 52 (2022) 122–131. https://doi.org/10.1080/24701556.2020.1862226

[20] M. Jaiswal, S. Srivastava, A review on sustainable approach of bioleaching of precious metals from electronic wastes, Journal of Hazardous Materials Advances 14 (2024) 100435. https://doi.org/10.1016/j.hazadv.2024.100435

[21] Y. Hwang, J.-K. Lee, J.-K. Lee, Y.-M. Jeong, S. Cheong, Y.-C. Ahn, S.H. Kim, Production and dispersion stability of nanoparticles in nanofluids, Powder Technol. 186 (2008) 145–153. 10.1016/j.powtec.2007.11.020

[22] A.Q. Malik, T. ul G. Mir, D. Kumar, I.A. Mir, A. Rashid, M. Ayoub, S. Shukla, A review on the green synthesis of nanoparticles, their biological applications, and photocatalytic efficiency against environmental toxins, Environmental Science and Pollution Research 30 (2023) 69796–69823. https://doi.org/10.1007/s11356-023-27437-9

[23] S. Yadav, T. Nadar, J. Lakkakula, N.S. Wagh, Biogenic synthesis of nanomaterials: bioactive compounds as reducing, and capping agents, in: Biogenic Nanomaterials for Environmental Sustainability: Principles, Practices, and Opportunities, Springer, 2024: pp. 147–188. https://doi.org/10.1007/978-3-031-45956-6_6

[24] B. Mughal, S.Z.J. Zaidi, X. Zhang, S.U. Hassan, Biogenic nanoparticles: Synthesis, characterisation and applications, Applied Sciences 11 (2021) 2598. https://doi.org/10.3390/app11062598

[25] M.J. Haque, M.M. Bellah, M.R. Hassan, S. Rahman, Synthesis of ZnO nanoparticles by two different methods & comparison of their structural, antibacterial, photocatalytic and optical properties, Nano Express 1 (2020) 10007. 10.1088/2632-959X/ab7a43

[26] Z. Vasiljevic, J. Vunduk, D. Bartolic, G. Miskovic, M. Ognjanovic, N.B. Tadic, M.V. Nikolic, An Eco-friendly approach to ZnO NP synthesis using Citrus reticulata Blanco peel/extract: Characterization and antibacterial and photocatalytic activity, ACS Appl. Bio Mater. 7 (2024) 3014–3032. https://doi.org/10.1021/acsabm.4c00079

[27] W.L.F. Armarego, Purification of laboratory chemicals, Butterworth-Heinemann, 2017.

[28] M. Karimi, A.M.H. Shabani, S. Dadfarnia, Deep eutectic solvent-mediated extraction for ligand-less preconcentration of lead and cadmium from environmental samples using magnetic nanoparticles, Microchimica Acta 183 (2016) 563–571. https://doi.org/10.1007/s00604-015-1671-9

[29] S. Kulkarni, H.N. Akolkar, V.M. Khedkar, R. Ramasamy, K.R. Mahanwar, N.R. Darekar, Biogenic-based Metal Nanomaterials for Sustainable Engineering Applications, CRC Press, 2025.

[30] G. Gupta, A.K. Kaur, A. Kumar, A Review on Nyctanthes arbortristis Linn an important traditional Plant of Herbal Medications, World Journal of Pharmaceutical Sciences (2021) 160–169. https://wjpsonline.com/index.php/wjps/article/view/96

[31] N. Rani, S. Rani, H. Patel, S. Yadav, M. Saini, S. Rawat, K. Saini, Characterization and investigation of antioxidant and antimicrobial activity of zinc oxide nanoparticles prepared using leaves extract of Nyctanthes arbor-tristis, Inorg. Chem. Commun. 150 (2023) 110516. https://doi.org/10.1016/j.inoche.2023.110516

[32] M. Ramesh, M. Anbuvannan, G. Viruthagiri, Green synthesis of ZnO nanoparticles using Solanum nigrum leaf extract and their antibacterial activity, Spectrochim. Acta A Mol. Biomol. Spectrosc. 136 (2015) 864–870. https://doi.org/10.1016/j.saa.2014.09.105

[33] A. Suresh, L. Jayakumar, Experimental Study on Mechanical, Thermal Conductivity, Wear, and Water Absorption Behaviour of Calotropis gigantea Stem Fiber/Citrus Maxima ZnO Reinforced Epoxy Composites, Silicon (2026) 1–16. https://doi.org/10.1007/s12633-025-03598-9

[34] J.S. Roy, S. Morency, Y. Messaddeq, Ultrafast cleaning of methylene blue contaminated water accelarating photocatalytic reaction rate of the BiVO4 nanoflakes under highly intense sunlight irradiation, J. Photochem. Photobiol. 7 (2021) 100037. https://doi.org/10.1016/j.jpap.2021.100037

[35] B.M. Ashwin, A. Yardily, M.S. Dennison, Microwave-assisted green synthesized ZnO nanoparticles: an experimental and computational investigation, Discover Applied Sciences 7 (2025) 1–20. https://doi.org/10.1007/s42452-025-06563-8

[36] X. Yu, X. Qi, S. Li, H. Fang, Y. Bai, L. Li, D. Liu, Z. Chen, W. Li, C. Liang, Transcriptome analysis of light-regulated monoterpenes biosynthesis in leaves of Mentha canadensis L., Plants 10 (2021) 930. https://doi.org/10.3390/plants10050930

[37] A. Munitz, M.J. Kaufman, M. Nahmany, N. Derimow, R. Abbaschian, Microstructure and mechanical properties of heat treated Al1. 25CoCrCuFeNi high entropy alloys, Materials Science and Engineering: A 714 (2018) 146–159. https://doi.org/10.1016/j.msea.2017.12.084

[38] Z.G. Umar, M.E. Abalaka, S.Y. Daniyan, H. Babayi, A.A. Adeniyi, Physicochemical and bio-metabolite characterizations of chitosan isolated from American cockroach (Periplaneta americana) and cricket (Acheta domesticus), (2022). http://irepo.futminna.edu.ng:8080/jspui/handle/123456789/17004

[39] M. Usman, A. Ahmed, B. Yu, Q. Peng, Y. Shen, H. Cong, Photocatalytic potential of bio-engineered copper nanoparticles synthesized from Ficus carica extract for the degradation of toxic organic dye from waste water: growth mechanism and study of parameter affecting the degradation performance, Mater. Res. Bull. 120 (2019) 110583. 10.1016/j.materresbull.2019.110583

[40] R. Patwa, S. Rohilla, J. Saini, P. Singh, Optimized ZnO/ZnS/Ag nanocomposites for UV-assisted degradation of methylene blue: A photocatalytic investigation, Ceram. Int. (2025). https://doi.org/10.1038/s41598-024-82764-2

[41] A.N. Kumar, M. Balakrishna, U. Desai, R. Rakshith, K.M. Ambika, P. Soumya, C.R. Ravikumar, S.S. Vadivu, N. Naik, Solution combustion synthesis of ZnO doped CuO nanocomposite for photocatalytic and sensor applications, Sci. Rep. 15 (2025) 338. https://doi.org/10.1016/j.ceramint.2025.07.277

[42] T. Varadavenkatesan, E. Lyubchik, S. Pai, A. Pugazhendhi, R. Vinayagam, R. Selvaraj, Photocatalytic degradation of Rhodamine B by zinc oxide nanoparticles synthesized using the leaf extract of Cyanometra ramiflora, J. Photochem. Photobiol. B 199 (2019) 111621.

[43] L. Qin, C. Shing, S. Sawyer, P.S. Dutta, Enhanced ultraviolet sensitivity of zinc oxide nanoparticle photoconductors by surface passivation, Opt. Mater. (Amst). 33 (2011) 359–362.

[44] U. Koch, A. Fojtik, H. Weller, A. Henglein, Photochemistry of semiconductor colloids. Preparation of extremely small ZnO particles, fluorescence phenomena and size quantization effects, Chem. Phys. Lett. 122 (1985) 507–510. https://doi.org/10.1016/0009-2614(85)87255-9

[45] M.M. Khan, N.H. Saadah, M.E. Khan, M.H. Harunsani, A.L. Tan, M.H. Cho, Potentials of

Costus woodsonii leaf extract in producing narrow band gap ZnO nanoparticles, Mater. Sci. Semicond. Process. 91 (2019) 194–200. https://doi.org/10.1016/j.mssp.2018.11.030

[46] N. Pantidos, L.E. Horsfall, Biological synthesis of metallic nanoparticles by bacteria, fungi and plants, J. Nanomed. Nanotechnol. 5 (2014) 1. http://dx.doi.org/10.4172/2157-7439.1000233

[47] A.A. Barzinjy, H.H. Azeez, Green synthesis and characterization of zinc oxide nanoparticles using Eucalyptus globulus Labill. leaf extract and zinc nitrate hexahydrate salt, SN Appl. Sci. 2 (2020) 991. https://doi.org/10.1007/s42452-020-2813-1

[48] S.G. Pandya, J.P. Corbett, W.M. Jadwisienczak, M.E. Kordesch, Structural characterization and X-ray analysis by Williamson–Hall method for Erbium doped Aluminum Nitride nanoparticles, synthesized using inert gas condensation technique, Physica E Low. Dimens. Syst. Nanostruct. 79 (2016) 98–102. https://doi.org/10.1016/j.physe.2015.12.013

[49] M.A. Ismail, K.K. Taha, A. Modwi, L. Khezami, ZnO nanoparticles: Surface and X-ray profile analysis, J. Ovonic Res 14 (2018) 381–393.

[50] S. Narayanan, M.S. Begum, G. Manikandan, M. Yuvashree, Green synthesis strategy for producing doped and undoped ZnO nanoparticles: their photocatalytic studies for industrial dye degradation, Water Science and Technology 84 (2021) 2958–2967.https://doi.org/10.2166/wst.2021.308

[51] B. Kumar, K. Smita, L. Cumbal, A. Debut, Green approach for fabrication and applications of zinc oxide nanoparticles, Bioinorg. Chem. Appl. 2014 (2014) 523869. https://doi.org/10.1155/2014/523869

[52] K. Aroosh, M. Javed, N. Hussain, A. Alhujaily, S. Iqbal, M.T. Alotaibi, M. Faizan, M.S. Khan, A. Bahadur, M.A. Qayyum, Construction of Te-ZnO@ Sg-C3N4 heterojunction nanocomposites for the efficient removal of methylene blue, antifungal activity, and adsorption of Cr (VI) ion, Adsorption Science & Technology 2023 (2023) 6736182. https://doi.org/10.1155/2023/6736182

[53] T. Mekedes, Musa acuminata peel extract assisted green Synthesis of ZnO/CuO Nanocomposite for Photocatalytic Degradation of Methylene Blue Dye, (2020).

[54] V. Rajendar, Y. Raghu, B. Rajitha, C.S. Chakra, K. V Rao, S.H. Park, Synthesis, characterization, and photocatalytic behaviour of nanocrystalline zno, tio 2 and zno/tio 2 nanocomposites., Journal of Ovonic Research 13 (2017).

[55] A. Negash, S. Mohammed, H.D. Weldekirstos, A.D. Ambaye, M. Gashu, Enhanced photocatalytic degradation of methylene blue dye using eco-friendly synthesized rGO@ ZnO nanocomposites, Sci. Rep. 13 (2023) 22234. https://doi.org/10.1038/s41598-023-48826-7

[56] L. Chen, I. Batjikh, J. Hurh, Y. Han, Y. Huo, H. Ali, J.F. Li, E.J. Rupa, J.C. Ahn, R. Mathiyalagan, Green synthesis of zinc oxide nanoparticles from root extract of Scutellaria baicalensis and its photocatalytic degradation activity using methylene blue, Optik (Stuttg). 184 (2019) 324–329. https://doi.org/10.1016/j.ijleo.2019.03.051

[57] A.N. Abdulqodus, A.F. Abdulrahman, S.H. Mostafa, A.A. Kareem, S.M. Hamad, S.M. Ahmed, M.A. Almessiere, D. Shaikhah, Green synthesis of ZnO nanoparticles: effect of pH on morphology and photocatalytic degradation efficiency, Applied Physics A 131 (2025) 720. https://doi.org/10.1007/s00339-025-08874-4